To be presented at the 1990 American Control Conference, San Diego, May 23-25

Approximate Minimum-Time Trajectories for Two-link Flexible Manipulators

G.R. Eisler, D.J. Segalman, R.D. Robinett
Engineering Analysis Department
Sandia National Laboratories†, Albuquerque, New Mexico

Abstract

The method of recursive quadratic programming has been used to generate approximate minimum-time tip trajectories for two-link semi-rigid and flexible manipulator movements in the horizontal plane. The manipulator is modeled with an efficient finite-element scheme for an n-link, m-joint system with bending only in the horizontal-plane. Constraints on the trajectory include boundary conditions on position and energy for a rest-to-rest maneuver, straight-line tracking between boundary positions, and motor torque limits. Trajectory comparisons utilize a change in the link stiffness to compare a semi-rigid configuration to a flexible one. The level of bending flexibility necessary to excite significant modal behavior is demonstrated. Applied torques for minimum-time maneuvers are shown to be very similiar between configurations and retain much of the qualitative character of rigid-body slewing motion.

Introduction

Trajectory planning is essential in budgeting the actuator efforts of a manipulator to maximize productivity. A variety of approaches has been advanced for rigid manipulator control, taking advantage of the fact that all or some of the controls take the form of switching functions between actuator bounds. Bobrow used an intuitive approach to generate optimal switching controls, as well as proving the boundedness of the controls [1]. Weinreb and Meier used calculus of variations approaches to incorporate control bounds in the problem formulation [2][3]. In a second study, Bobrow used numerical optimization to generate spline fits to the switching controls [4].

Pure switching functions do not lend themselves to maintaining tip accuracy for non-rigid structures. One would hope that the applied controls do take advantage of the bounds to maximize performance, but a clear analytical directive for this does not exist at the present time.

In filling this void, parameter optimization techniques can provide approximate optimal performance solutions for systems driven by complex, highly nonlinear dynamic models with arbitrary equality or inequality constraints. Of these solution techniques, the Recursive Quadratic Programming algorithm [5], embodied in the code VF02AD, has proven to be a robust tool for a variety of aerospace applications, and will be used in this study [6][7][8]. The primary drawback to this or other numerical optimization methods is the dependancy on accurate gradient approximations of the performance index and constraints with respect to the parameters.

The ensuing discussion initially describes the structural dynamics model of the manipulator,

†This work performed at Sandia National Laboratories was supported by the U.S. Department of Energy under contract number DE-AC04-76DP00789.

---

followed by the optimal control problem and parameterization of the controls. It concludes with the results of a computational experiment.

The manipulator structure modeled in this study has been fabricated as a two-link, cantilever arrangement constrained to slew in the horizontal plane. Tall, thin links are used to minimize vertical plane droop. The hub or joint-1 actuator slews both links, an interlink motor, and tip payload. The interlink or joint-2 actuator located at the end of link-1 slews the second link and the tip payload. The joint-1/joint-2 actuator torque ratio used in this study is 4/1. The complete manipulator is about 0.5 meters (m) tall and 1.2m long (Fig.1).

The Structural Model

There is extensive literature discussing the difficulties of simulating the vibrations of rotating structures[9] [10] [11]. The problem arises from kinematics that are of second order importance in nonrotating problems, but become of first order importance in the presence of rotational accelerations. Additonally, there are constraints inherent to the flexible link problem which must be satisfied: motions occur entirely in a horizontal plane; one end of the chain of links is attached to a stationary hub; and each flexible link is inextensible.

The full kinematics are retained by expressing the configuration as functions of convected coordinates (i.e., coordinates attached to the arm) and measuring distance from the hub. This is a traditional approach in nonlinear elasticitity [12]. Further, the kinematic variables are selected so that all geometric constraints (fixed hub, planar motion, and non-extension) are automatically satisfied.

Since motions are assumed to occur entirely in a plane, it is also assumed that the elastic lines of the links as well as the mass centers of the cross sections all lie in the same plane. Each cross section is identified by its arc-length distance from the hub, so that the orientation of the center of the cross section s at time t is

$$\vec{\beta}(s,t) = cos(\theta(s,t))\vec{i} + sin(\theta(s,t))\vec{j}$$

The vector $\vec{\beta}(s,t)$ is the unit tangent along the arm at s, and the basis vectors $\vec{i}$ and $\vec{j}$ are fixed in space.

The location of the center of cross section s (relative to a space fixed frame) at time t is obtained by integration of the above unit tangent vector:

$$\vec{x}(s,t) = \int_0^s \vec{\beta}(\hat{s},t)d\hat{s}$$

Similarly, the velocity at the cross section s at time t is obtained by integration of the time derivative of $\vec{\beta}(s,t)$:

$$\dot{\vec{x}}(s,t) = \int_0^s \dot{\theta}(\hat{s},t)\vec{\gamma}(\hat{s},t)d\hat{s}$$

where

$$\vec{\gamma}(s,t) = -sin(\theta(s,t))\vec{i} + cos(\theta(s,t))\vec{j}$$

The above description of configuration - entirely in terms of $\theta(s,t)$ - causes all of the geometrical constraints to be satisfied automatically. Additionally, the above description expresses the configuration in terms of one unknown field (θ), instead of the more conventional two or three fields (x, y, & θ).

The governing dynamics equations are derived using these kinematics and a frame-invariant variational method - Hamilton's principle. A finite element discretization is used to cast the resulting integro-differential equations for $\theta(s,t)$ and its first and second derivatives into a system

of fully-coupled, nonlinear algebraic equations. Particularly important for the current application is the observation made below that since all spatial integrals are with respect to the convected coordinate, s, those integrals are configuration-independent and need be done only once. The nonlinearities remain, and a new nonlinear system must be solved at each time step, but the time consuming quadrature process can be done in advance of the dynamics simulation.

Hamilton's principle states

$$\delta \int_{t_1}^{t_2} \left[KE(\hat{t}) - SE(\hat{t}) + WE(\hat{t}) \right] d\hat{t} = 0 \tag{1}$$

where KE is kinetic energy, SE is strain energy, WE is external work, and $\hat{t}$ a dummy variable. The governing equations of motion of the flexible structure are obtained by consideration of the integrand alone:

$$\delta KE(t) - \delta SE(t) + \delta WE(t) = 0 \tag{2}$$

for all $t_1 \leq t \leq t_2$.

The kinetic energy is that of the flexible links plus that of all concentrated masses and concentrated moments of inertia:

$$KE(t) = \frac{1}{2} \int_0^L \rho(s)\, \dot{\vec{x}}(s,t) \cdot \dot{\vec{x}}(s,t) ds + \frac{1}{2} \sum_{k=1}^{masses} M_k\, \dot{\vec{x}}(s_k,t) \cdot \dot{\vec{x}}(s_k,t) + \frac{1}{2} \sum_{l=1}^{inertias} I_l\, \dot{\theta}(s_l,t) \cdot \dot{\theta}(s_l,t)$$

In the above, $\rho(s)$ is the mass per unit length measured along the length of the arm; M_k is the magnitude of the kth point mass; s_k is the convected coordinate of the kth point mass; I_l is the magnitude of the lth point moment of inertia; and s_l is the convected coordinate of the lth point moment of inertia.

The strain energy is that of the flexible links:

$$SE(t) = \frac{1}{2} \int_0^L \kappa(s,t) \frac{\partial \vec{\beta}(s,t)}{\partial s} \cdot \frac{\partial \vec{\beta}(s,t)}{\partial s} ds$$

where $\kappa(s,t)$ is the curvature at cross section s at time t.

The virtual work due to externally imposed torques is:

$$\delta WE(t) = \int_0^L \vec{\tau}(s,t) \cdot (\vec{\beta}(s,t) \times \delta\vec{\beta}(s,t)) ds \tag{3}$$

where $\vec{\tau}(s,t)$ is the imposed torque.

Discretization along the rod of the above energy terms is obtained by discretizing the tangent vector $\vec{\beta}$ as:

$$\vec{\beta}(s,t) = \sum_{n=1}^{nodes} \vec{\beta}_n(t) p_n(s)$$

where the shape functions, p_n, are nonzero over intervals that are small relative to the anticipated radii of curvature. The above condition on the support of the basis functions is necessary to assure compliance with the condition of nonextension. The shape functions used in the computer code described below were the traditional tent-shaped basis functions. Since these shape functions are bases for β the resulting elements take on piece-wise circular shape, with continuous slope between the elements. Joints are defined by co-locating two nodes so that the tangent vector $\vec{\beta}$ may be discontinuous there.

The resulting energies are:

$$KE(t) = \frac{1}{2} \sum_{m=1}^{nodes} \sum_{n=1}^{nodes} \dot{\theta}_m(t)\dot{\theta}_n(t)\vec{\gamma}_m(t) \cdot \vec{\gamma}_n(t) M_{m,n} \tag{4}$$

$$SE(t) = \frac{1}{2} \sum_{m=1}^{nodes} \sum_{n=1}^{nodes} \vec{\beta}_m(t) \cdot \vec{\beta}_n(t)\, K_{m,n} \tag{5}$$

and

$$\delta WE(t) = \sum_{m=1}^{nodes} \vec{\tau}_m(t) \cdot \vec{k}\delta\theta_m \qquad (\vec{k} = \vec{i} \times \vec{j}) \tag{6}$$

where

$$M_{m,n} = \int_0^L \rho(s)\, q_m(s)\, q_n(s) ds + \sum_{k=1}^{masses} M_k\, q_m(s_k)\, q_n(s_k) + \sum_{l=1}^{inertias} I_l\, p_m(s_l)\, p_n(s_l) \ ,$$

$$q_m(s) = \int_0^s p_m(\hat{s}) d\hat{s} \ , \qquad K_{m,n} = \int_0^L \kappa(s)\, p'_m(s)\, p'_n(s) ds \ ,$$

nodes is the number of nodes, δ_K is the Kronecker delta function, $\hat{s}$ is a dummy variable, p'_m and p'_n are derivatives with respect to s of p_m and p_n, and $\vec{\tau}_m$ is the net torque applied at node m. Then the time-independent matrices, $M_{m,n}$ and $K_{m,n}$ are the topological mass and stiffness matrices, respectively.

After appropriate integration by parts, the integrand of equation 2 becomes:

$$\sum_{n=1}^{nodes} \delta\theta_m(-\vec{\gamma}_m(t) \cdot \ddot{\vec{\beta}}_n(t) M_{m,n} - \vec{\gamma}_m(t) \cdot \vec{\beta}_n(t) K_{m,n} + \vec{k} \cdot \vec{\tau}_n(t)\delta_k(m,n)\,) = 0 \tag{7}$$

for all nodes m. In the above equation, τ_n is the external torque applied at node n. After $\ddot{\vec{\beta}}_n(t)$ is expanded:

$$\ddot{\vec{\beta}}_n(t) = \ddot{\theta}_n(t)\vec{\gamma}_n(t) + (\dot{\theta}_n(t))^2 \vec{\beta}_n(t)$$

and Equation 7 is invoked for all $\delta\theta_m$, a complete set of *nodes* second order equations in the *nodes* unknowns, $\ddot{\theta}_n$, results in:

$$\vec{k} \cdot \vec{\tau}_m(t) = \sum_{n=1}^{nodes} \left[\vec{\gamma}_m(t) \cdot \vec{\gamma}_n(t)\ddot{\theta}_n(t) M_{m,n} - \vec{\gamma}_m(t) \cdot \vec{\beta}_n(t)(\dot{\theta}_n(t))^2 M_{m,n} + \vec{\gamma}_m(t) \cdot \vec{\beta}_n(t) K_{m,n}\right] \tag{8}$$

The above problem formulation lends itself to rapid numerical calculation. It involves only one unknown field, automatically satisfies all constraints, and requires only one evaluation of element mass and stiffness matrices Ref. [13].

Optimal Trajectory Shaping

The principal goal in this study is to combine the physics of the structure with optimization techniques to generate actuator torque histories for accomplishing a useful task with minimal degradation in performance. A secondary objective is to minimize the work of a feedback controller, which will be needed to compensate for modeling errors.

A minimum-time tip trajectory was chosen for investigation, as a candidate for maximizing productivity for a give repetitive task. Constraints on such a trajectory include: completing a

rest-to-rest maneuver, tracking a specified path $(x(t), y(t))_{tip}$, slewing between specified endpoints $[(x(t_o), y(t_o)),\ (x(t_f), y(t_f))]_{tip}$, and not exceeding actuator torque limits $\tau_{1,2_{max}}$.

The configuration initially starts at rest. Driving a flexible structure to rest at the final time, t_f, necessitates end constraints on both kinetic and potential or strain energies $(KE(t_f), SE(t_f))$. The chosen path is a straight line and actuator torque limits are constants. Torque limits can be integrated naturally into the controls as

$$\tau_{1,2}(t) = |\tau_{1,2_{max}}| \sin \alpha_{1,2}(t)$$

where $\alpha(t)$ is a free variable. This form assumes that the two-sided limits on $\tau_{1,2}(t)$ are of the same magnitude. Final accelerations are also to be zeroed. The problem can be restated as

minimize: $J = t_f$

subject to:
- finite element model
- input actuator torques, $\tau_{1,2}(t)$
- known initial conditions

constrained by:

$$\begin{bmatrix} \\ C_j(t_f) = 0 \\ \\ \\ \\ \end{bmatrix}_{j=1,7} = \begin{bmatrix} x_{tip}(t_f) - x_{specified}(t_f) \\ y_{tip}(t_f) - y_{specified}(t_f) \\ \int_0^{t_f} [y_{tip}(x_{tip}(t)) - y_{line}(x_{tip}(t))]^2\, dt \\ KE(t_f) \\ SE(t_f) \\ \ddot{\theta}_{joint\ 1}(t_f) \\ \ddot{\theta}_{joint\ 2}(t_f) \end{bmatrix}$$

Note that the equality tracking constraint, C_3 is formulated as an integral. In addition, equality constraints on energy are *point* constraints. Both of these items will have profound effects on the example trajectories to be generated.

Parameterization of the Controls

To approximate optimum system performance from the aforementioned structural model, a suitable parameterization of the controls, $\tau_{1,2}(t)$ via α, is necessary. For this study, the simplest case was chosen. Tabular values of α, at equal-spaced fixed times, t_i, for both joints were chosen as parameters, or

$$\alpha_1(t_i),\ \alpha_2(t_i),\quad i = 1, n \qquad 0 \le t_i \le t_f,$$

which results in $2n$ control parameters.

However, since the final time is changing due to minimization, the loss of control history definition would result if the times at which the control parameters are defined remain fixed in an absolute sense. To correct this, $\alpha_{1,2}$ were specified at equally-spaced, nondimensional *node* points, $\zeta_i = t_i/t_f$, where

$$\alpha_1(\zeta_i),\ \alpha_2(\zeta_i),\quad i = 1, n \qquad 0 \le \zeta_i \le 1,$$

This allows the torque histories to "stretch" naturally over the trajectory length. Using this modification, it is necessary to add t_f as a parameter also, resulting in $2n + 1$ control parameters to be found. Linear interpolation was used to compute $\alpha(\zeta)$ between the node values.

Numerical derivatives of the performance index, t_f, and the constraints, $C_j(t_f)$, provided to VF02AD are central finite-difference approximations. In computing these approximations, complete trajectories (or integrations of Eq.8) are computed using the current nominal t_f to produce perturbed $C_j(t_f)$ values. Since derivatives are computed over the current *fixed* t_f, the derivatives, $\partial t_f/\partial(\alpha_{1,2})_i = 0$, and only the derivatives, $\partial C_j(t_f)/\partial(\alpha_{1,2})_i \neq 0$. Obviously, both $t_f, C_j(t_f)$ gradients with respect to t_f, evaluated over the current nominal torque histories, are nonzero, (where $\partial t_f/\partial t_f = 1.$).

Results

The following finite-element structural model for the manipulator was used to produce the sample trajectories.

ITEM	LENGTH (m)	MASS (kg)	EI (newton-m^2)
joint-1 bracket	.0635	.545	10^5
link-1	.5040	.640	10^2,10^3
1st joint-2 bracket + joint-2	.1070	5.415	10^5
2nd joint-2 bracket	.1040	.830	10^5
link 2	.4890	.313	10^2,10^3
Totals:	1.2675	7.743	

Brackets were modeled with 1 element and considered rigid ($EI = 10^5$), and links were modeled with 3 elements for a total of 9 elements. The two values of stiffness, EI, for links 1,2 represent the trajectory comparison for this study. Point moments of inertia were used to define mass distribution for the brackets. No payload was used in this comparison. The joints were assumed to have no compliance or damping.

The two trajectories, computed on a CRAY-XMP, were integrated for 100 time steps, where $\Delta t = .01t_f$. Trajectory evaluations for gradient computations executed in 0.75 secs. The $\alpha(\zeta)$ histories for each joint were composed of 21 tabular values, where $\Delta\zeta = .05$. Torque bounds were chosen as $\pm 16, \pm 4$ newton-m (n-m) for joints 1 and 2. The path to be tracked for this study was the line connecting (x, y) pairs, (0.0,1.13) and (1.13,0.0). A composite of the slew motion for the "flexible" case ($EI_{links} = 100$ newtons-m^2) is given in Fig.2. The parameterized torque histories that created this slew represent 500 iterations of VF02AD after initialization with parameter solution values from the rigid-link solution. The tip path traced is essentially straight, but does contain some small ripples - a result of the integral statement of the tracking constraint, $C_3(t_f)$.

Figure 3 graphically depicts the difference between the semi-rigid and flexible links. Shown is the angular velocity of the finite-element node adjacent to joint 1. The frequency of vibration for $EI_{links} = 100$ is about 17 Hz. An examination of Fast Fourier Transforms (FFTs) of the finite-element output of the system disturbed about the initial, midtime, and final positions, shows this to be one of the lower modes. Note the low angular velocity of the semi-rigid system after $t/t_f = 0.9$, implying that a significant amount of time is being expended in order to bring the system to "rest". This phenomenon is definitely at odds with purely rigid system behavior. The $KE(t_f) = 0$ and angular acceleration constraints impose a nearly zero final angular velocity for both configurations. Note that t_f for both cases is approximate the same.

Fig.4 shows the τ_1 profiles. These retain much of the bounded appearance of switching functions for purely rigid configurations. However, they begin and end near zero instead of the bounds (± 16

n-m). These torque profiles exhibit very similiar behavior except at the intermediate switch point. Other than the slight ripples for the $EI_{links} = 100$ case, this phenomena is the major difference between the configurations. Note the abruptness of the controls near the end in an attempt to quiet the structure. The τ_2 torques in Fig.5 show minimal activity for most of the trajectory, except close to the end in order to accomplish the rest state. Again, very little "torquing" difference is noted for the order of magnitude change in link stiffness between configurations.

The straight-line tracking error in millimeters (mm) is shown in Fig.6. Both torque histories appear to limit the error to less than ± 0.5 mm except near the end where the error momentarily "escapes" to about 2 mm. One drawback to the integral formulation is that it can relax tracking performance in isolated parts of the trajectory, yet yield a reasonably low residual (≈ 0) for $C_3(t_f)$. It may be necessary to add interior point constraints to decrease this error.

The peak kinetic energy of the flexible structure at $t/t_f \approx 0.45$ is, not surprisingly, higher than the semi-rigid one as shown in Fig.7. It is interesting that KE appears to be devoid of oscillatory behavior in both cases. It also manifests strikingly similiar behavior between trajectories except at the peak, which would correspond to the intermediate switch point shown in Fig.4. Note again the rest phase of the trajectories above $t/t_f = 0.9$. Strain energy is shown in Fig.8. This again displays the contrast first seen in Fig.3. The semi-rigid structure produces relatively little strain (however does contain a high frequency ripple), while the flexible-link configuration again contains the 17 Hz mode with a sizable increase in energy magnitude. Note the major changes in both cases, mirroring the sharp τ_1 changes in Fig.4. Also, note the enforcement of the $SE(t_f) = 0$ point constraint at the end.

Conclusions

A robust, parameter optimization tool has been successfully employed to generate actuator torque histories for approximate, minimum-time slewing maneuvers containing continuous and point constraints for a 2-link flexible manipulator. The parameters, or actuator torques, for each link were tabular values at fixed node points during the maneuver. Perturbations were made to each parameter to approximate final time and constraint gradients. The efficient formulation of the finite-element model made the numerical optimization procedure a realistic endeavor.

The accuracy of the straight-line tip tracking was excellent. For the trajectory used in this study, joint-1 applied most of the input in a manner resembling rigid-link torquing. Torque histories were very similiar between configurations even though link stiffness varied by an order of magnitude, and the t_f performance index was virtually the same. Energy and acceleration constraints were effective in bringing the structure nearly to rest at t_f. It was also demonstrated that final energy constraints do not preclude vibrations during the slew. The intended production use of the manipulator will dictate whether or not this is a hindrance.

References

[1] J.E. Bobrow, S. Dubowksy and J.S. Gibson, "Time-Optimal Control of Robotic Manipulators along Specified Paths", *Int. J. Robotics Res.*, Vol 4.,no.3, Fall 1985

[2] Weinreb, A., Bryson, A.E., "Optimal Control of Systems with Hard Control Bounds", *IEEE Transactions on Automatic Control*, Vol.AC-30, No.11, Nov. 1985, pp.1135-1138

[3] E.B. Meier and A.E. Bryson, "An efficient algorithm for time-optimal control of a two-link manipulator,", in AIAA conference on Guidance, Navigation, and Control, Monterey, CA, Aug 1987, pp 204-212.

[4] Bobrow, J.E., "Optimal Robot Path Planning Using the Minimum-Time Criterion", *IEEE J. Robotics and Automation*, Vol.4, No.4, August 1988

[5] Powell, M.J.D., "A Fast Algorithm for Nonlinearly Constrained Optimization Calculations", *Proceedings of the Biennnial Conference on Numerical Analysis*, Springer-Verlag, Berlin, 1978, pp.144-157

[6] Eisler, G.R., Hull, D.G., "Maximum Terminal Velocity Turns at Nearly Constant Altitude", *Journal of Guidance, Control, and Dynamics*, Vol.11, No.2, March-April 1988, pp.131-136

[7] Outka, D.E., "Parameter Optimization Capability in the Trajectory Code PMAST", SAND86-2917, Sandia National Laboratories, Albuquerque, 1987

[8] Robinett, R.D., "A Unified Approach to Vehicle Design, Control, and Flight Path Optimization", The Center for Strategic Technology, Texas A&M University, SS87-1, 1987

[9] J. C. Simo and L. Vu-Quoc 'The role of non-linear theories in transient dynamic analysis of flexible structures', *Journal of Sound and Vibration, Vol. 119*, 1987, pp 487-508.

[10] T. R. Kane, R. R. Ryan, and A. K. Banerjee, 'Dynamics of a cantilever beam attached to a moving base', *Journal of Guidance, Control and Dynamics, Vol. 10*, 1987, pp 139-151.

[11] S. Hanagud and S. Sarkar, 'Problem of the dynamics of a cantilever beam attached to a moving base', *Journal of Guidance, Control and Dynamics*, Vol. 12, 1989, pp 438-441.

[12] A. E. Green and W. Zerna, *Theoretical Elasticity*, Clarendon Press, Oxford, 1954.

[13] D. J. Segalman, 'A Mathematical Formulation for the Rapid Simulation of a Flexible Multilink Manipulator' SAND89-2308, Sandia National Laboratories, Albuquerque, New Mexico

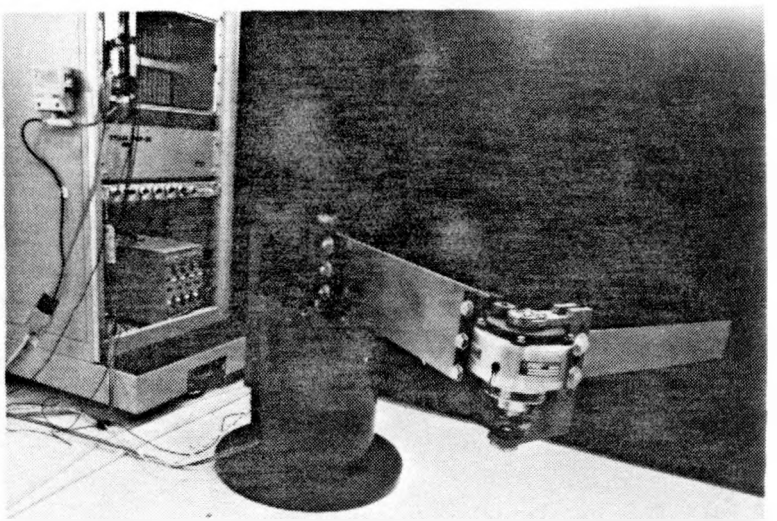

Figure 1: Sandia two-link manipulator

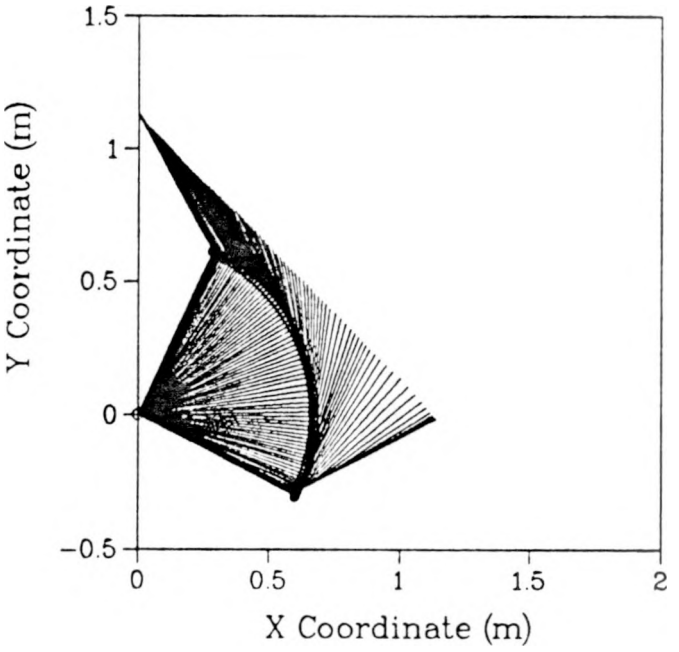

Figure 2: Composite motion for $EI_{links} = 100$

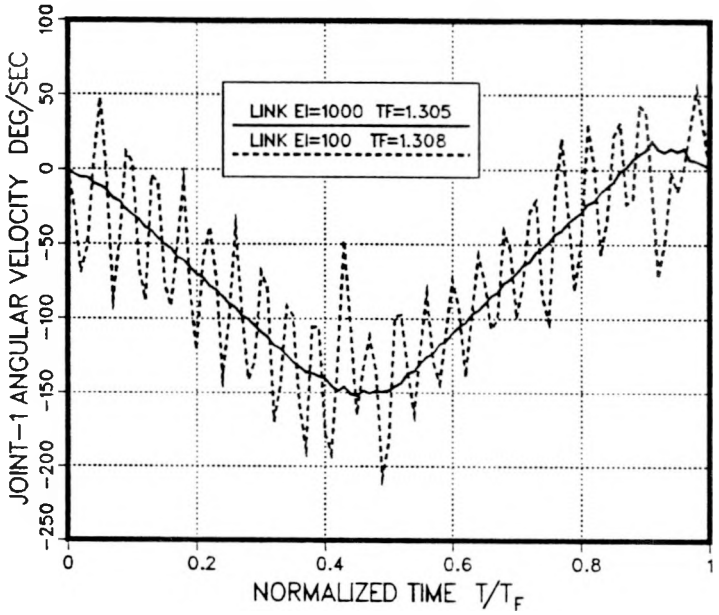

Figure 3: Joint 1 node angular velocity

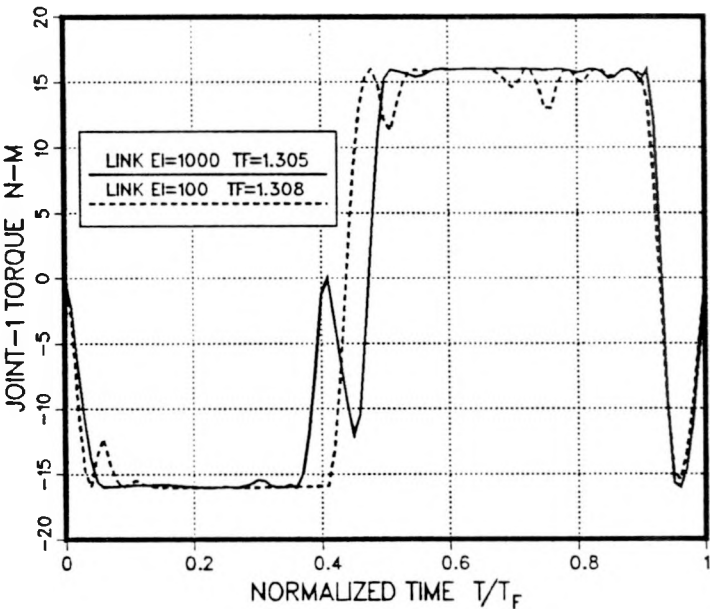

Figure 4: τ_1 joint torque histories

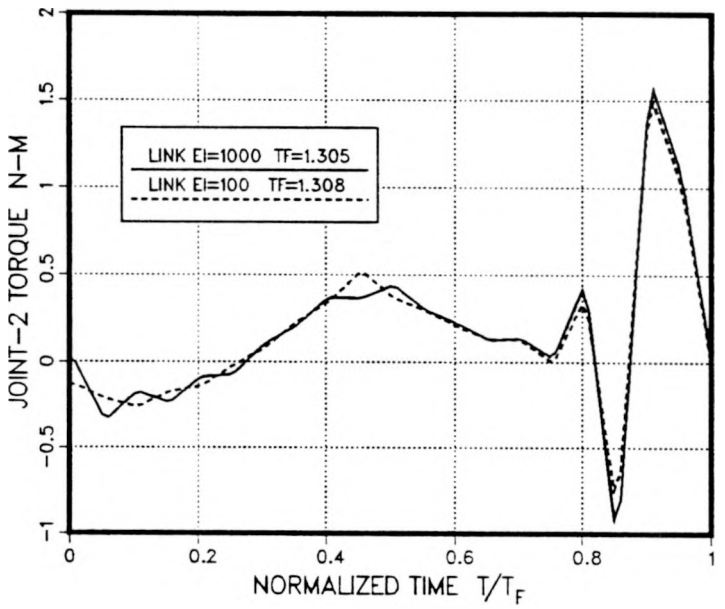

Figure 5: τ_2 joint torque histories

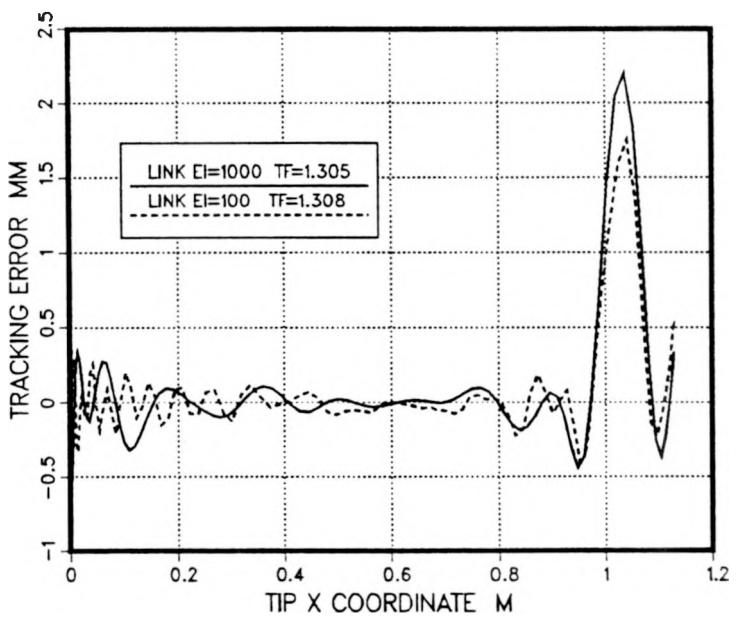

Figure 6: Straight-line tracking error

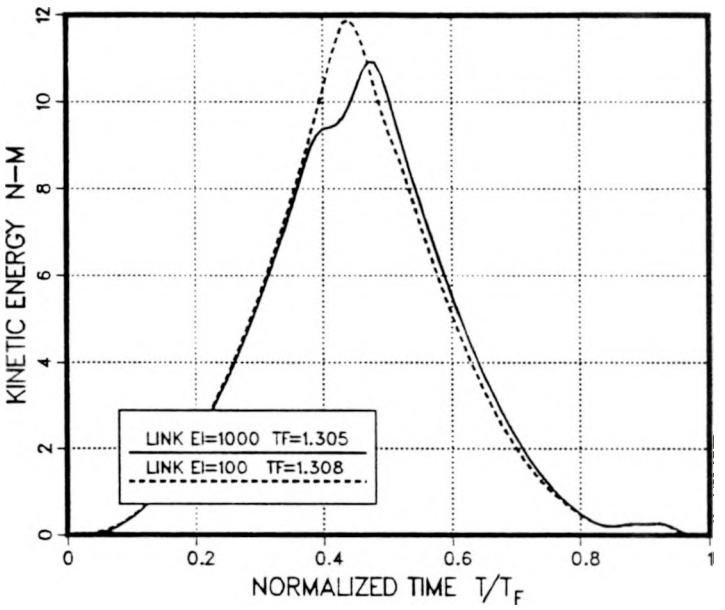

Figure 7: Kinetic energy histories

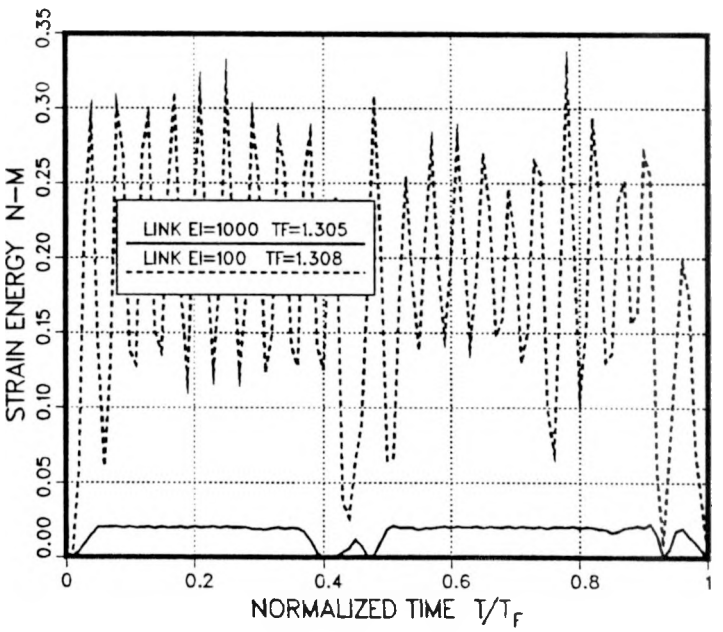

Figure 8: Strain energy histories